A Voxel-Based Morphometric Study of Ageing
in 465 Normal Adult Human Brains

Catriona D. Good,* Ingrid S. Johnsrude,† John Ashburner,* Richard N. A. Henson,*,‡
Karl J. Friston,* and Richard S. J. Frackowiak*

*Wellcome Department of Cognitive Neurology, Institute of Neurology, Queen Square, London; †Now at MRC Cognition
and Brain Sciences Unit, 15 Chaucer Road, Cambridge; and ‡Institute of Cognitive Neuroscience,
University College London, 17, Queen Square, London WC1N 3BG United Kingdom

Voxel-based-morphometry (VBM) is a whole-brain, unbiased technique for characterizing regional cerebral volume and tissue concentration differences in structural magnetic resonance images. We describe an optimized method of VBM to examine the effects of age on grey and white matter and CSF in 465 normal adults. Global grey matter volume decreased linearly with age, with a significantly steeper decline in males. Local areas of accelerated loss were observed bilaterally in the insula, superior parietal gyri, central sulci, and cingulate sulci. Areas exhibiting little or no age effect (relative preservation) were noted in the amygdala, hippocampi, and entorhinal cortex. Global white matter did not decline with age, but local areas of relative accelerated loss and preservation were seen. There was no interaction of age with sex for regionally specific effects. These results corroborate previous reports and indicate that VBM is a useful technique for studying structural brain correlates of ageing through life in humans. © 2001 Academic Press

Key Words: ageing; normal; MRI; voxel based morphometry.

INTRODUCTION

There is compelling evidence from post mortem and *in vivo* studies that the brain shrinks with age, but accurate quantification of the specific patterns of age-related atrophy has proved elusive. It is unclear whether there are predictable common patterns of ageing or whether individual human brains respond to the ageing process idiosyncratically. Postmortem analysis of mammalian brains suggest that there may be a gradient of ageing from the association areas to the primary sensory regions, with the former showing the most prominent correlations between age and atrophy (Flood and Coleman, 1988). Many postmortem and *in vivo* brain imaging studies have addressed the ageing issue, but many of these are limited by methodological

constraints such as small sample size. Postmortem analyses of brain structure depend on factors such as the interval between death and fixation, the timing of measurements (Last and Tompsett, 1953; Messert, 1972; Miller *et al.,* 1980), and the inclusion or exclusion of brain stem structures and meninges (which can be difficult to control), and hence vary across studies. Furthermore, if brain weight is related to body height, the progressive increase in height over the past century may limit the applicability of conclusions from the significant fraction of postmortem studies that were conducted in the last century (Miller and Corsellis, 1977). A number of *in vivo* imaging studies have attempted to quantify age-related change in whole brain volume, grey matter, white matter and CSF compartments, using CT, 2-D MRI, and more recently high resolution MRI morphometry. Apart from the more obvious limitations of small cohort studies and earlier imaging techniques (Schwartz, 1985), as well as variability in reporting absolute or fractional volumes, the majority of these studies have been based on manual or semiautomated region of interest guided measurements (Raz *et al.,* 1997; Filipek *et al.,* 1994; Pfefferbaum *et al.,* 1994; Luft *et al.,* 1999; Xu *et al.,* 2000), which may be inherently biased. This bias is introduced by the small number of regions and metrics used in classical morphometrics that are insensitive to changes elsewhere in the brain. A number of unbiased whole brain techniques are emerging due to the improved resolution of structural MRI scans and the development of sophisticated image processing tools: The simplest methods apply rigid body registration within subject, e.g., Fox and Freeborough (1996), compared age-related changes over 1 year in a small group of patients with Alzheimer's disease and controls using a semiautomated rigid body coregistration technique, and subsequently they showed little change in nine elderly controls over 1 year using a fluid registration technique (Freeborough and Fox, 1998). Guttmann *et al.* (1998) used a fully automated segmentation technique to

evaluate the effects of age on tissue compartments, but provided no information with regional specificity within these compartments. More complex models are required to register images from larger cohorts into a common stereotactic space using linear or nonlinear forms of spatial normalization enabling region by region comparisons. For example, voxel-based morphometry (VBM) allows a voxel-wise comparison of spatially normalized images, deformation-based morphometry (DBM) and tensor-based morphometry (TBM) use the deformation fields derived from spatial normalization to make comparisons. The former to identify differences in relative positions of brain structures and the latter to detect local shape differences. There is a large body of literature on various forms of such methods (e.g., Ashburner *et al.,* 1998; Christensen *et al.,* 1997; Davatzikos *et al.,* 1996, 1998; Guimond *et al.,* 2000; Thompson, 1997), but as yet ageing data is not available from large subject groups.

Recently Resnick *et al.* (2000) showed cross sectional and 1 year longitudinal age changes in a relatively large group (*n* = 116) of elderly subjects using a semi-automated brain extraction technique followed by fully automated segmentation, nonlinear normalization and automatically determined Talairach "boxels" of interest.

The great variety in morphometry methodologies may in part explain the conflicting literature on linear and nonlinear patterns of tissue change, the effect of sex and the heterogeneic response of various compartments of the brain to ageing.

In this cross sectional study of a relatively large group of normal adults (*n* = 465), we applied VBM in order to characterize and quantify age-related change in the human brain on a voxel-by-voxel basis. This facilitates not only the assessment of separate brain compartments, namely grey and white matter and CSF, but also subregions within these compartments. The standard (simple) technique of VBM has been used in a number of studies with relatively small subject groups. In this study with a substantially larger subject group we reveal potential problems of the standard technique and the need for further improvements to minimise error while maximizing sensitivity. The differences between the standard (Wright *et al.,* 1995; Ashburner and Friston, 2000) and optimized methods will be highlighted in the methods section.

METHODS

Subjects

Approval for the study was obtained from the joint ethics committee of the National Hospital for Neurology and Neurosurgery and the Institute of Neurology, UCL. The study group was selected from a population of 1761 normal volunteers who responded to advertisements and were scanned at the Wellcome Department of Cognitive Neurology between February 1998 and December 1999. All subjects with any neurological, medical, psychiatric condition, or migraine were excluded. Inclusion criteria included: (1) Normal MRI brain as determined by an experienced neuroradiologist (CDG). Any MRI scans with structural abnormalities, prominent normal variants (e.g., mega cisterna magna, cavum septum pellucidum) or technical artefacts were excluded; (2) no history of alcohol intake of more than 30 units/week or intake of more than 10 units within 48 h prior to scanning (a unit of alcohol is equal to 10 ml of pure alcohol and is roughly equivalent to a glass of wine (125 ml) or a single measure of spirits (25 ml); (3) no history of severe head trauma requiring medical attention; (4) no history of cognitive difficulties; (5) no history of treated hypertension. 465 subjects met all the inclusion criteria. They comprised 29 left-handed females (aged 18–75, median 31), 171 right-handed females (aged 18–79, median 28), 38 left-handed males (aged 20–59, median 33), and 227 right-handed males (aged 17–67, median 26).

Structural MRI Scanning Protocol

Magnetic resonance imaging was performed on a 2 Tesla Siemens MAGNETOM Vision scanner. A 3-D structural MRI was acquired on each subject using a T-1-weighted MPRAGE sequence (TR/TE/TI/NEX 9.7/4/600/1, flip angle 12°, matrix size 256 × 192, FOV 256 × 192, yielding 120 sagittal slices and a slice thickness of 1.5 mm with in-plane resolution of 1 × 1 mm.

Data Analysis

Data were analyzed on a Sun Ultra 60 workstation (Sun Microsystems, Mountain View, CA) using MATLAB 5.3 (MathWorks, Natick, MA) and SPM 99 (Wellcome Dept. Cogn. Neurol, London; http://www.fil.ion.ucl.ac.uk/spm) (Friston *et al.,* 1995a).

Preprocessing of Structural Data

In this section we first describe the standard method of VBM which we used initially for grey and white matter and CSF preprocessing and for the creation of templates. We then highlight the need for an optimized method, and finally we describe the various steps of the optimized method for grey and white matter.

Before preprocessing, all the structural images were checked for artefacts and the center point was placed on the anterior commissure.

Standard VBM Protocol (Fig. 1a)

Template creation. First, an anatomical template was created from a subgroup of 120 normal subjects (60 females and 60 males matched for age and handedness), with a mean age and age range matched to the entire study group imaged on the same MRI scanner

with the same scanning parameters, in order to reduce any scanner-specific bias and provide a template appropriate to the population sample. This involves spatially normalizing (see below for details) each structural MRI to the ICBM 152 template (Montreal Neurological Institute), which is derived from 152 normal subjects and approximates the Talairach space. The normalized data are then smoothed with an 8-mm full-width at half-maximum (FWHM) isotropic Gaussian kernel, and a mean image (the template) is created.

Spatial normalization. All 465 structural MRI scans (in native space) were transformed to the same stereotactic space by registering each of the images to the same template image, using the residual sum of squared differences as the matching criterion. The first step in spatial normalization involves estimating the optimum 12-parameter affine transformation to match images (Ashburner *et al.,* 1997). A Bayesian framework is used, whereby the maximum *a posteriori* (MAP) estimate of the spatial transformation is made using prior knowledge of the normal variability in brain size. The second step accounts for global non-linear shape differences, which are modeled by a linear combination of smooth spatial basis functions (Ashburner and Friston, 1999). A masking procedure is used to weight the normalization to brain rather than nonbrain tissue. The spatially normalized images are resliced with a final voxel size of approximately $1.5 \times 1.5 \times 1.5$ mm^3.

Segmentation. Scans were then segmented into grey matter, white matter, CSF, and other nonbrain partitions. SPM segmentation employs a mixture model cluster analysis to identify voxel intensities matching particular tissue types (grey matter, white matter and CSF) combined with an *a priori* knowledge of the spatial distribution of these tissues in normal subjects, derived from probability maps. The segmentation step also incorporates an image intensity non-uniformity correction (Ashburner and Friston, 2000) to address image intensity variations caused by different positions of cranial structures within the MRI head coil.

Smoothing. The normalized, segmented images are smoothed using a 12-mm FWHM isotropic Gaussian kernel. This conditions the data to conform more closely to the Gaussian field model underlying the statistical procedures used for making inferences about regionally specific effects. Smoothing also has the effect of rendering the data more normally distributed (by the central limit theorem). The intensity in each voxel of the smoothed data is a locally weighted average of grey matter density from a region of surrounding voxels, the size of the region being defined by the size of the smoothing kernel (Ashburner and Friston, 2000).

Motivation for Optimization

Inspection of segmented images from the simple preprocessing procedure described above often showed several small areas of missegmented nongrey matter voxels. For example, on segmented grey matter images, voxels from the dural venous sinuses, scalp fat, petrous apices, and diploic space are often misclassified as grey matter (Fig. 2). This has implications if there are systematic differences in skull size and shape or scalp thickness among study groups, especially if the groups are large, as in this study. For example, in a separate VBM analysis of sex effects on grey matter (the subject of a separate manuscript), large clusters of significant differences that were not ascribable to grey matter change were seen along the course of the venous sinuses and outside the brain margins. This error is removed by the introduction of additional preprocessing steps to exclude nonbrain voxels prior to normalization and subsequent segmentation. New features of the optimized method include (i) a fully automatic brain extraction technique, (ii) study-specific grey/white matter templates. We also describe a modulation step to incorporate volume changes during normalization into the analysis. This modulation procedure allowed us to assess both regionally specific age-related changes in grey/white matter volume and concentration (i.e., density). Effectively this protocol employs a recursive version of segmentation, extraction, and normalization operators.

Optimized VBM Protocol (Fig. 1b)

Creation of a separate grey and white matter templates. Separate grey and white matter templates were created by averaging all the 465 smoothed normalized grey/white matter images from the simple VBM protocol described above. We chose to create the optimised templates from the whole subject group rather than a subset in order to further reduce any potential bias for spatial normalization.

Segmentation and extraction of a brain image. This is a fully automated procedure to remove scalp tissue, skull, and dural venous sinus voxels. This procedure initially involves segmentation of the original structural MR images (in native space) into grey and white matter images, followed by a series of fully automated morphological operations for removing unconnected non-brain voxels from the segmented images (erosion followed by conditional dilation). The resulting images are extracted grey and white matter partitions in native space.

Normalization of grey/white matter images. The extracted segmented grey/white matter images are normalized to the grey/white matter templates thus preventing any contribution of nonbrain voxels and affording optimal spatial normalization of grey/white matter. There is, however, a caveat: the initial segmentation (implicit in the brain extraction step) is performed on affine-normalized images (in native space), but the probability maps, used as Bayesian priors for segmentation, are in stereotactic space. Segmentation
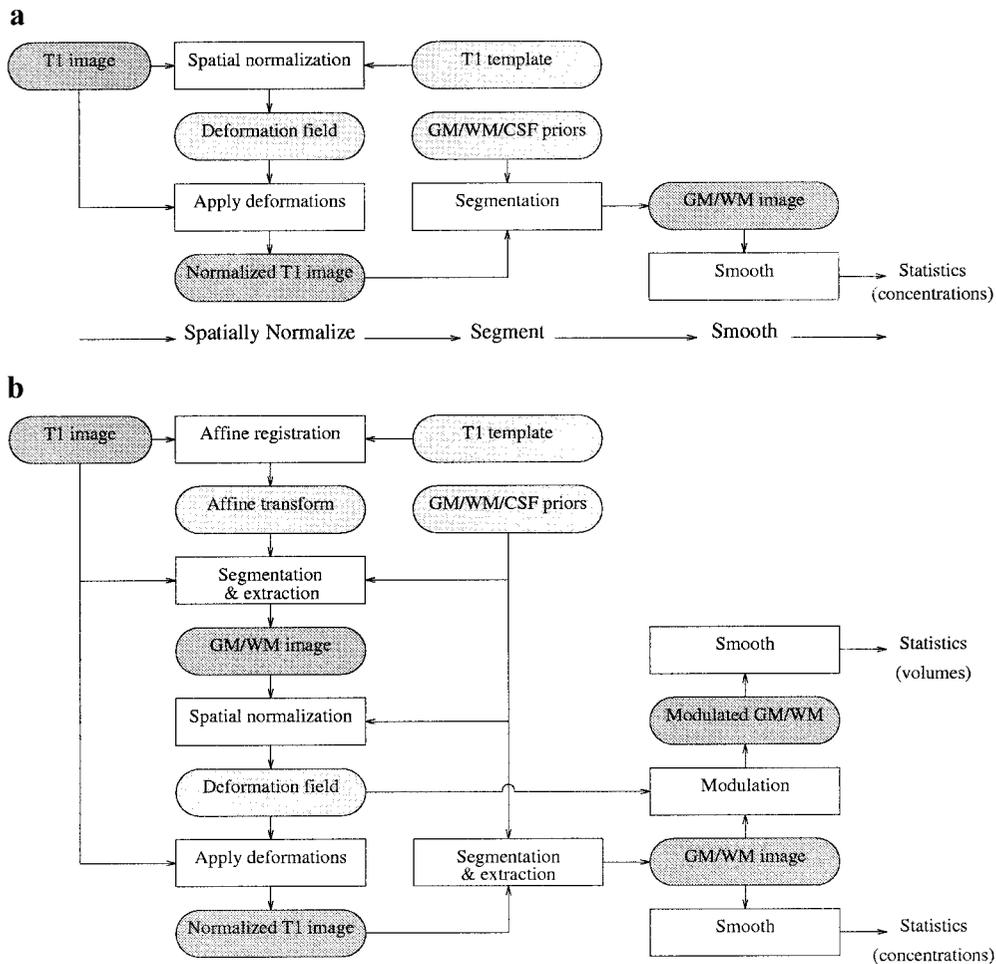
a

b

FIG. 1. Flow diagram showing the various preprocessing steps for the standard (a) and optimized (b) protocols.

of fully normalized images is therefore preferable. In order to facilitate an optimal segmentation, the optimized normalization parameters are reapplied to the original, whole brain structural images (in native space).

Segmentation and extraction of normalized whole brain images. The optimally normalized whole brain structural images, which are now in stereotactic space, are then segmented into grey and white matter, CSF, and non-CSF partitions and subject to a second extraction of normalized segmented grey/white matter images. The brain extraction step is repeated at this stage because some nonbrain voxels from scalp, skull, or venous sinuses in the optimally normalized whole brain images could still remain outside the brain margins on segmented grey/white matter images.

Correction for volume changes (modulation). As a result of nonlinear spatial normalization, the volumes of certain brain regions may grow, whereas others may shrink. In order to preserve the volume of a particular tissue (grey or white matter or CSF) within a voxel, a further processing step is incorporated. This involves multiplying (or modulating) voxel values in the seg-

mented images by the Jacobian determinants derived from the spatial normalization step. In effect, an analysis of modulated data tests for regional differences in the absolute amount (volume) of grey matter, whereas analysis of unmodulated data tests for regional differences in concentration of grey matter (per unit volume in native space) (Ashburner and Friston, 2000). In this study we analyzed both modulated and unmodulated data.

Smoothing. As in the standard VBM method, each optimally normalized, segmented, modulated image is smoothed with a 12-mm FWHM kernel.

Validation of the technique. Details on the evaluation of the VBM segmentation technique, including evaluation of the nonuniformity correction and stability with respect to misregistration with the *a priori* images can be obtained in Ashburner and Friston (2000). Evaluation of the assumptions about normally distributed data are also detailed in this reference. In order to determine scan–rescan differences in tissue classification, we scanned 10 subjects twice on the same day. Each subject left the scanner room between scans, and the time interval between scans was ap-
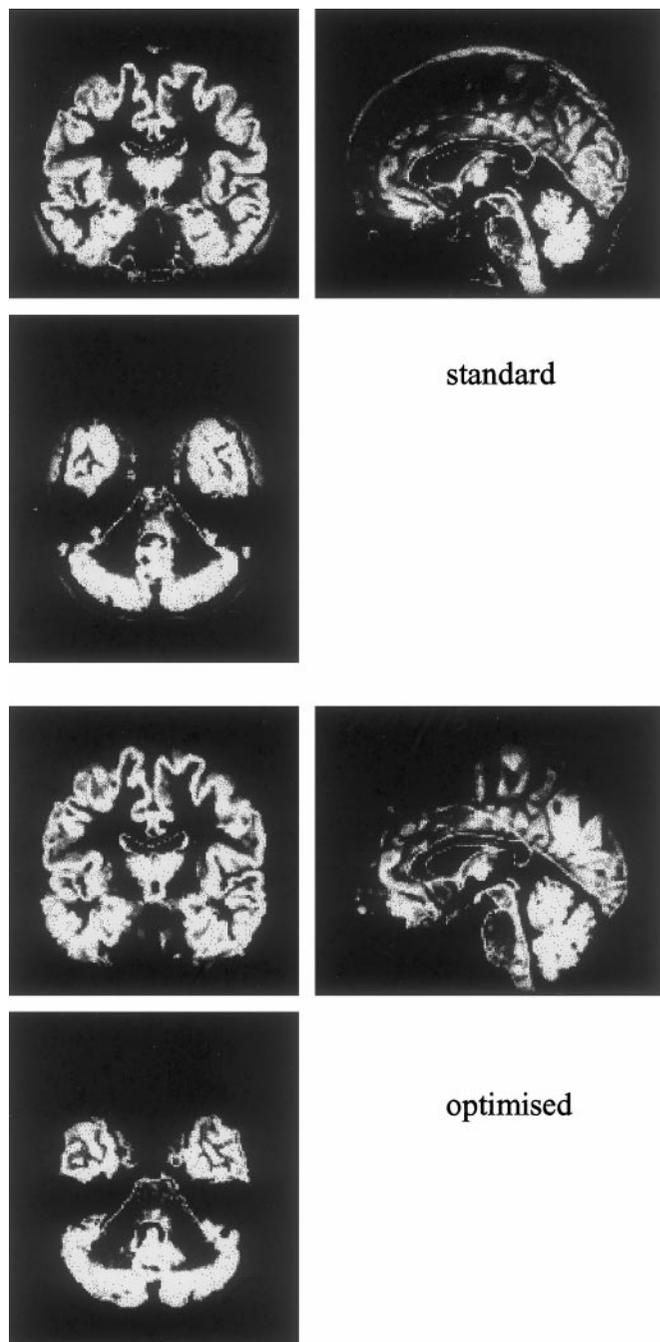
FIG. 2. Grey matter segmented images derived from the standard and optimised VBM techniques. Many nonbrain voxels can be seen in the dural venous sinuses, scalp fat, and diploic space in the grey matter segments derived from the standard technique, which are removed with the optimised technique.

proximately 15 min. For the standard VBM method, the coefficient of variation ($100 \times$ standard deviation of the differences/overall mean) for grey matter volume, white matter volume, CSF volume, and TIV were 0.45, 0.75, 1.07, and 0.16, respectively. For the optimized VBM method, the coefficients of variation for grey matter volume, white matter volumes, CSF volume, and

TIV were 0.41, 0.59, 1.07, and 0.17, respectively. These values show that tissue classification is highly reproducible using the both standard and the optimised VBM methods. Furthermore, a VBM statistical analysis using a paired t test design matrix yielded no significant regional differences between first and second scans, even with reduced corrected thresholds of 0.5. The standard VBM technique has been validated with independent region of interest measurements (Maguire *et al.,* 2000; Vharga-Khadem *et al.,* 1998) and we have recently validated the optimised VBM technique with an independent automated segmentation technique and region of interest measurements in groups of elderly healthy subjects and patients with Alzheimer's disease and semantic dementia (manuscript in preparation). Since no gold standard exists against which *in vivo* measurements can be compared and, furthermore, since variations in MRI protocols, normalization, and segmentation techniques can be expected to produce inconsistent data, reproducibility of a given technique is more important. In this regard the tissue classification technique used in this study yielded highly reproducible results.

Statistical Analysis

The normalized, smoothed, segmented data were analyzed using statistical parametric mapping (SPM99) employing the framework of the General Linear Model (Friston *et al.,* 1995a). Global effects of age were examined by multiple regression of summed voxel values of grey matter, white matter, CSF, and total intracranial volume (TIV) in a model including linear and quadratic expansions of age for both males and females. Significance levels for F statistics were set at $P < 0.05$.

Regionally specific differences in grey (and white) matter between groups were assessed statistically using a two-tailed contrast, namely testing for an increased or decreased probability of a voxel being grey (or white) matter. We tested for volumetric changes in grey or white matter by incorporating the modulation of segmented data. Concentration changes were assessed by using the segmented images directly. Normalization for global differences in voxel intensity across scans was effected by inclusion of the global mean voxel value (grey matter globals for the grey matter analysis and white matter globals for the white matter analysis) as a confounding covariate in an analysis of covariance (ANCOVA), while preserving regional differences in grey (and white) matter (Friston *et al.,* 1995a). Orthogonalized first-, second-, and third-order polynomial expansions of age were entered into the design matrix to determine the linear and nonlinear effects of age. Corrections for the search volume (and implicit multiple comparisons) in terms of the P values were made using Gaussian random field theory, which accommodates spatial correlations inherent in the data and is now established as the conventional

approach to inference in smooth spatially extended data (Friston *et al.,* 1995b; Worsley *et al.,* 1996). We assessed the goodness of fit of first, second and third order polynomial expansions using F maps or SPM{F} (Buchel *et al.,* 1996). Significance levels for the F statistics were set at $P < 0.05$, corrected for multiple comparisons. Significance levels for one-sided T statistics were set at $P < 0.025$, corrected.

RESULTS

Grey Matter

Global effects of age.   There was a decline of global grey matter volume with age (Fig. 3a); overall $R^2 = 0.489$. This involved cortical and deep gray matter structures and cerebellum diffusely and a similar pattern was observed when TIV was included as a confounding covariate. The linear coefficient (b1) was significant for both males, b1 $= -0.0039$, $F(1,458) = 58.7$, $P < 0.0001$, and females, b1 $= -0.0026$, $F(1,458) = 31.7$, $P < 0.0001$. Both quadratic coefficients failed to reach significance ($F < 1.06$, $P > 0.30$). The rate of decline was greater in males than females, a trend that approached significance, $F(1,458) = 3.54$, $P < 0.06$. The mean grey matter volume was significantly greater in males (0.829 liters) than females (0.747 liters), $F(1,458) = 239.85$, $P < 0.0001$. There was no effect of handedness on global grey matter volume, $F(1,458) < 1$. When absolute volumes were expressed as a fraction of TIV, a similar significant pattern of linear decline was noted for males ($P < 0.001$) and females ($P < 0.001$), although the increased decline in males was less marked, $F(1457) = 0.8$, $P = 0.17$. The mean fractional volume of grey matter was significantly greater for males than females ($P < 0.001$), although this was less pronounced than the absolute volume difference (Fig. 3b). The grey–white absolute volume ratio was 1.89 for females and 1.89 for males. The grey–white fractional volume ratio was 1.82 for females and 1.82 for males.

Regional effects of age.   Local areas of relative accelerated loss of grey matter volume (i.e., more than the global loss) were observed bilaterally in the superior parietal gyri, pre- and postcentral gyri, insula/frontal operculum, right cerebellum (posterior lobe), and anterior cingulate (Fig. 4a). Areas of relative accelerated loss of grey matter concentration were observed in the left middle frontal gyrus (F2), transverse temporal (Heschl's) gyri bilaterally, and left planum temporale (Fig. 4b). Areas of relative preservation (i.e., less than the global loss) of grey matter volume were noted symmetrically in the lateral thalami, amygdala, hippocampi, and entorhinal cortex (Fig. 4c). Areas of relative preservation of grey matter concentration were seen more diffusely in the thalami (Fig. 4d). Table 1 demonstrates the stereotactic coordinates corrected P and Z scores for grey matter analyses.

These local effects tended to be linear, with no improved fit to the data with inclusion of a second and/or third order polynomial term. There were no significant two- or three-way interactions with age and sex and handedness.

White Matter

Global effects of age.   There was no significant decline in white matter volume with age (Fig. 3c), overall $R^2 = 0.326$. The linear coefficients were not significant ($F < 1.05$, $P > 0.30$), though the quadratic coefficient approached significance for females, b2 $= 0.0004$, $F(1,468) = 3.65$, $P < 0.06$ (but not males, $F < 1$). The mean white matter volume was significantly greater in males (0.454 liters) than females (0.395 liters), $F(1,458) = 218$, $P < 0.0001$, but no other sex differences approached significance ($F < 1.27$). There was no effect of handedness on global white matter volume $F(1,458) < 1$. When white matter volume was expressed as a fraction of TIV, the quadratic coefficient was significant for females ($P < 0.01$), but not for males (Fig. 3d).

Regional effects of age.   There were local areas of relative accelerated loss of white matter volume bilaterally in frontal white matter, optic radiations (Fig. 5a), and posterior limbs of internal capsule, bordering on the ventrolateral thalamus. Local areas of accelerated decline of white matter concentration were seen bilaterally in posterior limbs of internal capsule, bordering on the lateral thalamus (Fig. 5b). Inspection of white matter segmented images (from the optimized preprocessing method) shows some lateral thalamus voxels classified as white matter (see Discussion). There were local areas of relative preservation of white matter volume bilaterally in the posterior frontal lobes (Fig. 5c), cerebellum, and right temporal lobe. Relative preservation of white matter concentration was noted bilaterally in the internal capsules, frontal, and posterior temporal/occipital white matter (Fig. 5d). Table 2 demonstrates the stereotactic coordinates of local maxima, corrected P and Z scores for the white matter analyses.

These local effects of age also tended to be linear, with no improved fit to the data with inclusion of second and/or third order terms, apart from two small foci of accelerated nonlinear decline in white matter concentration at the anterior aspect of both internal capsules. There were no significant two- or three-way interactions with age and sex and handedness.

CSF

Global effects of age.   There was a global increase in CSF volume with age (Fig. 3e), overall $R^2 = 0.377$. This involved the entire CSF compartment including the ventricles and surface sulci. A similar pattern was observed when TIV was included as a confounding covariate. The linear coefficient was significant for both

males, b1 = 0.0019, $F(1,458) = 39.1$, $P < 0.0001$, and females, b1 = 0.0018, $F(1,458) = 40.2$, $P < 0.0001$. The quadratic coefficient was significant for females, b2 = 0.0003, $F(1,458) = 5.53$, $P < 0.05$, but not males, $F < 1$. The mean CSF volume did not differ significantly between males (0.397 liters) and females (0.401 liters), $F(1,458) = 1.91$, $P = 0.22$, and no other sex differences approached significance, $F < 1.9$, $P > 0.16$. There was no significant effect of handedness on CSF volume $F(1,458) < 1$. When CSF was expressed as a fraction of TIV, the linear coefficients were significant for males ($P < 0.001$) and females ($P < 0.001$); and the quadratic coefficient was significant only for females ($P = 0.006$). There was also a significant difference in mean fractional volume of CSF, females more than males ($P < 0.001$) (Fig. 3f).

There was a slight but significant linear decline of TIV with age for males ($P = 0.008$) but not for females ($P = 0.282$). Both quadratic coefficients failed to reach significance. The rate of decline was greater in males than in females, a trend that approached significance, $F(1,457) = 1.9$, $P = 0.08$. The mean TIV was significantly greater for males than females ($P < 0.001$) (Fig. 3g).

Regional effects of age. Relatively little enlargement of the CSF space was seen in the pontine cistern, including its caudal extent around the medulla (Fig. 6a). Areas of accelerated enlargement of the CSF space were seen symmetrically in the chiasmatic and supracerebellar cisterns, cisterna magna, third ventricle, and the Sylvian and interhemispheric fissures (Fig. 6b). Regional effects of age tended to be linear with no improved fit of the data with inclusion of a second and/or third order polynomial expansion of age.
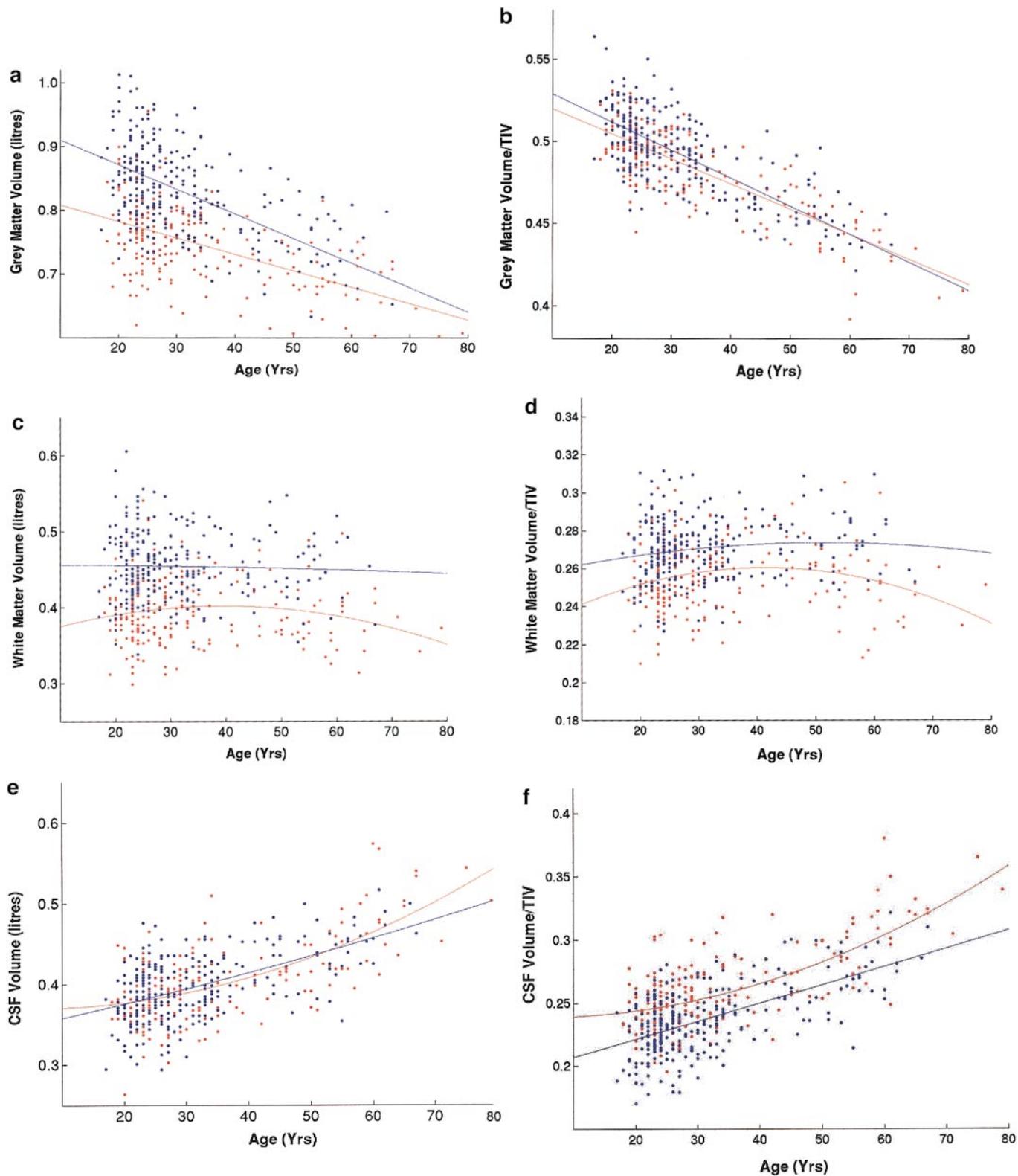
DISCUSSION

Subject Selection

This is a cross-sectional study in which structural age differences observed at a given time are used to make inferences about the ageing process. This approach has inherent limitations since there is potential for confounding age and cohort effects and, in particular, for secular bias, which can only be resolved by a longitudinal study. Haug (1985) points out that the increase in height due to secular acceleration is in the order of approximately 1 mm per year, and as body weight increases, so does brain weight. There has been a trend in the literature to report brain volumes as percentages of body height or total intracranial volume, and we have therefore provided data on absolute and fractional (as a fraction of TIV) brain volumes (Fig. 2). It is worth noting that there are subtle differences between the two, (as demonstrated in Figs. 3a–3f), which further explains the inconsistency in the literature on ageing. The major drawback of a longitudinal

study is the time it would take to acquire data from youth to senescence. It would also be practically impossible to maintain identical scanning parameters, thereby introducing systematic differences unassociated with ageing per se. Longitudinal studies thus tend to look at small time windows in the ageing process. Another difficult issue is the question of what constitutes a "normal" ageing population? We recruited volunteers responding to advertisements distributed around the university and local community, and the vast majority of volunteers were of European extraction. Most young and middle aged subjects were students or professionals with higher degrees, and the majority of elderly volunteers were motivated, high functioning individuals, many attending educational programs and thus probably not representative of the population at large. We excluded all volunteers with controlled hypertension, but since blood pressure rises with increasing age, we may have excluded "normal" elderly subjects, and this is reflected in our relatively small numbers of subjects in the seventh to ninth decades. We did not perform any cognitive tests on subjects, but we excluded subjects with any history of cognitive decline and all subjects completed a questionnaire as part of the recruitment process. If anything, our elderly population errs on the side of high cognitive functioning. We are currently setting up a study to look longitudinally at a smaller cohort of elderly subjects with comprehensive cognitive testing, functional and structural imaging.

Silent Brain Lesions

Deep white matter lesions are seen on magnetic resonance imaging in approximately one-third of asymptomatic elderly subjects (Fein *et al.,* 2000) and the significance of these remains unclear. Some reports have suggested an association between silent white matter lesions and coronary artery stenosis, hypertension, and cognitive performance. A CT- and MRI-based study using relatively crude region of interest measurements reported an association between silent white matter lesions and brain atrophy (Yamano *et al.,* 1997). The bulk of evidence suggests, however, that they are merely frequent incidental findings in the elderly, with no link to significant central nervous system pathological processes. A recent MRI study on the sex effects of age-related changes in brain structure (Xu *et al.,* 2000) specifically excluded all subjects with silent brain lesions, citing the CT study mentioned above. In our study, we specifically did not exclude healthy subjects whose MRIs showed a few small hyperintense white matter foci, because we consider these to be normal findings, and exclusion of such subjects would misrepresent the normal ageing population.
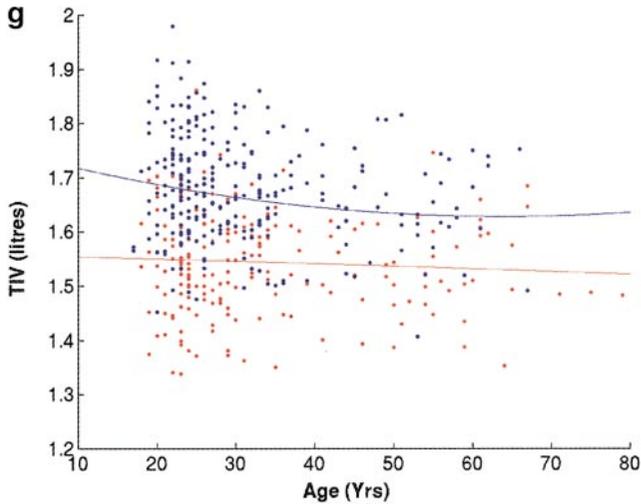
g

FIG. 3.—*Continued*

Global Effects of Age: Grey Matter, White Matter, and CSF

Many neuropathological studies show that normal ageing is characterised by a substantial and extensive loss of neurons in the cerebral cortex, although this is controversial, with recent stereological investigations indicating little neuronal loss with normal ageing (e.g., Peters *et al.,* 1998; Gomez-Isla, 1996, 1997), and some reports suggesting that alterations in cerebral white matter and subcortical neuronal loss may be the predominant effect of age (Guttman *et al.,* 1998). Our data concur with those neuropathological and previous CT and MRI morphometry studies that suggest ageing predominantly and substantially affects the grey matter (Pfefferbaum *et al.,* 1992, 1994; Lim *et al.,* 1992; Jernigan *et al.,* 1991; Schwartz, 1985). In particular, our data suggest a linear decline in grey matter in concordance with Pfefferbaum *et al.* (1994), and we observed this pattern of decline for absolute and fractional grey matter volumes. Others have suggested accelerated ageing in the later decades of life, and since our data included relatively few subjects over 65 years, and furthermore our elderly subjects could be considered to be "super normal," we could be missing this nonlinear trend.

The majority of structural MRI data indicate that although significant microstructural changes are seen in cerebral white matter (Raz *et al.,* 1997; Wahlund *et al.,* 1990), significant total white matter volume loss is not expressed (Jernigan *et al.,* 1991; Pfefferbaum *et al.,* 1992, 1994; Raz *et al.,* 1993). Our data are consistent with this finding. This phenomenon may be due to concomitant factors with opposing influence: the loss of myelin associated with ageing (Ansari and Loch, 1975) may reduce white matter bulk, whereas the simultaneous expansion of the capillary network and swelling of perivascular spaces (Meier-Ruge *et al.,* 1992) may enlarge white matter bulk. In accordance with previous CT and MRI literature, we observed an increase in the CSF compartment with age, best described by a linear function. We noted a small but significant decline in TIV with age in males and a smaller nonsignificant trend in females, which most probably reflects the secular trend of increasing head size over the last century. The mean absolute grey–white matter volume ratio was 1.89, and the mean fractional grey–white volume ratio was 1.82. Grey–white matter ratios vary widely in the literature, for example postmortem and *in vivo* studies, using a variety of methodologies, report ratios in a wide range from approximately 3–1.1, dependent on age (e.g., Caviness *et al.,* 1996; Guttmann *et al.,* 1998; Pfefferbaum *et al.,* 1994; Resnick *et al.,* 2000).

Regional Effects of Age

Our data support the theory of a heterogeneic response of various compartments of the brain to ageing. We observed accelerated loss of grey matter volume symmetrically in both parietal lobes (angula gyri), pre- and postcentral gyri, insula, and anterior cingulate cortex. We also observed accelerated loss of grey matter concentration in the left middle frontal gyrus, left planum temporale and transverse temporal gyri bilaterally. There was relative preservation of grey matter volume symmetrically in the amygdala, hippocampi, entorhinal cortices, and lateral thalami, with relative preservation of grey matter concentration more diffusely in the thalami. This is in accordance with previous work showing a predominant age effect in the parietal lobes (Resnick *et al.,* 2000) and prefrontal grey matter (Raz *et al.,* 1997); a smaller effect in fusiform,

FIG. 3. (a) Scatter plot of total grey matter volume (liters) against age (years) for 465 normal subjects (females in red, males in blue). The best fitting linear regression curves for females and males are superimposed. (b) Scatter plot of fractional grey matter volume (/TIV) against age (years) for 465 normal subjects (females in red, males in blue). The best fitting linear regression curves for females and males are superimposed. (c) Scatter plot of total white matter volume (litres) against age (years) for 465 normal subjects (females in red, males in blue). The best fitting quadratic regression curves for females and males are superimposed. (d) Scatter plot of fractional white matter volume (/TIV) against age (years) for 465 normal subjects (females in red, males in blue). The best fitting quadratic regression curves for females and males are superimposed. (e) Scatter plot of total CSF volume (liters) against age (years) for 465 normal subjects (females in red, males in blue). The best fitting quadratic regression curves for females and males are superimposed. (f) Scatter plot of fractional CSF volume (/TIV) against age (years) for 465 normal subjects (females in red, males in blue). The best fitting quadratic regression curves for females and males are superimposed. (g) Scatter plot of TIV against age (years) for 465 normal subjects (females in red, males in blue). The best fitting quadratic regression curves for females and males are superimposed.
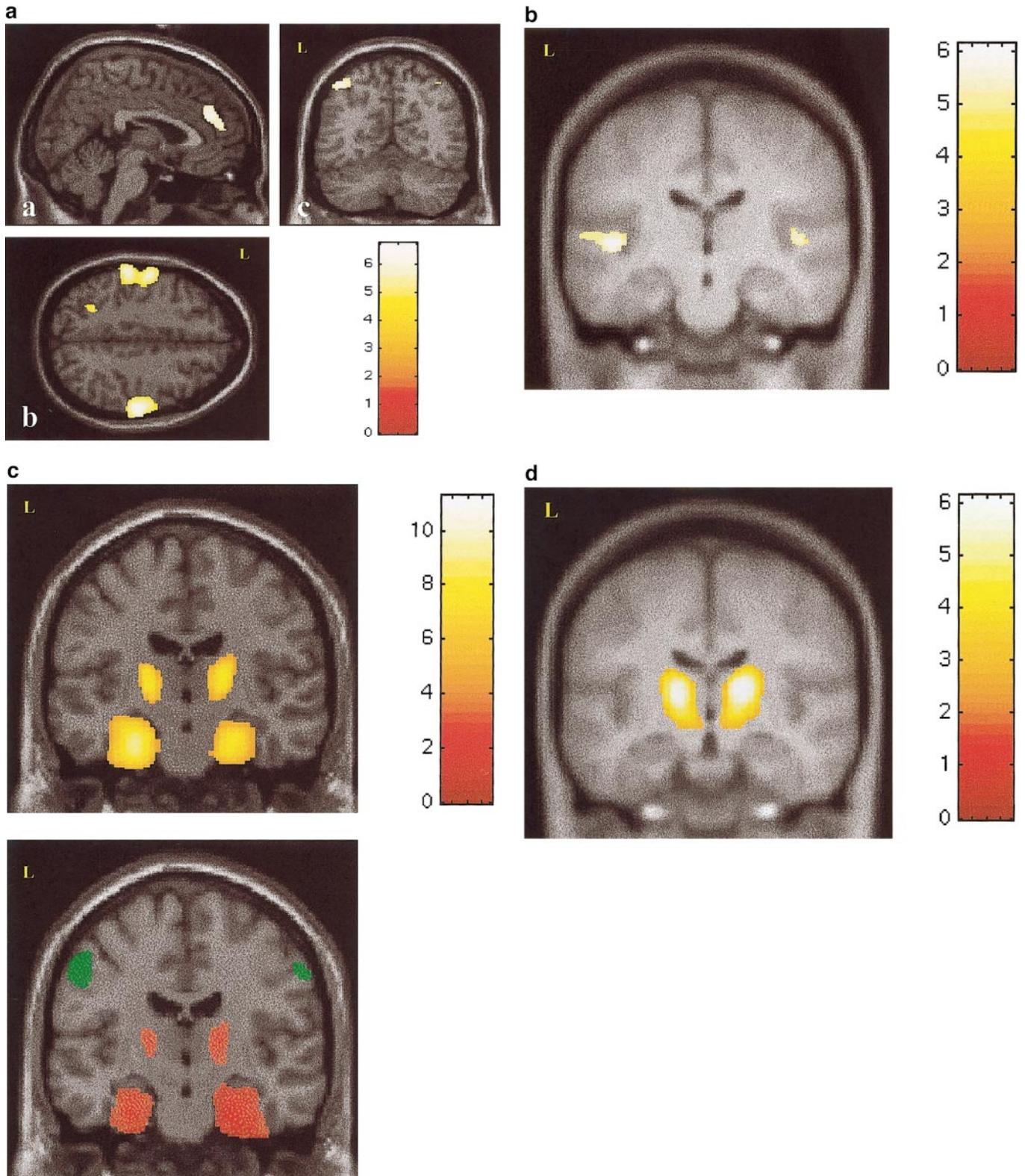
FIG. 4. (a) Grey matter volume: (modulated) negative correlation with age. Regions of relative accelerated loss of grey matter volume from 465 normal subjects superimposed on a normalized structural image in the sagittal plane (a), axial plane (b), and coronal plane (c). The color bar represents the T score. Significant voxels ($P < 0.025$ corrected) are seen bilaterally in the anterior cingulate (a), bilateral pre- and postcentral gyri (b), and bilateral angular gyri (b, c). The significant cerebellar and anterior insula voxels are not shown. (b) Grey matter concentration: (unmodulated) negative correlation with age. Regional areas of relative accelerated loss of grey matter concentration from 465 normal subjects superimposed on the whole brain template derived from all subjects. The color bar represents the T score. Significant voxels ($P < 0.025$ corrected) are seen bilaterally in the transverse temporal (Heschl's) gyri and left planum temporale. (c) Grey matter volume:

TABLE 1

x	y	z	Z	P(corrected)	Location

x	y	z	Z	P(corrected)	Location
			Grey matter: modulated negative correlation		
−42	57	54	6.44	<0.0001	L angular gyrus
42	−58	54	5.35	<0.0001	R angular gyrus
2	42	26	6.17	<0.0001	Anterior cingulate sulcus
−40	21	10	6.07	<0.0001	L anterior insula
42	4	15	6.06	<0.0001	R anterior insula
62	−20	40	6.44	<0.0001	R pre and post central gyri
−57	−28	45	5.88	<0.0001	L post central gyrus
−54	−9	50	6.14	<0.0001	L precentral gyrus
31	−90	−34	5.36	<0.0001	R cerebellum (posterior lobe)
			Grey matter: unmodulated negative correlation		
−52	21	38	5.7	<0.0001	L middle frontal gyrus
−46	−20	2	6	<0.0001	L Heschl's gyrus/planum temporale
45	−16	2	5.7	<0.0001	R Heschl's gyrus
−2	15	−9	5.51	0.002	Subcallosal gyrus
			Grey matter: modulated positive correlation		
−27	−4	−21	>8	<0.0001	L amygdala/hippocampus
26	−3	−22	>8	<0.0001	R amygdala/hippocampus
			Grey matter: unmodulated positive correlation		
15	−17	9	>8	<0.0001	R thalamus
−14	18	8	>8	<0.0001	L thalamus
40	−80	24	5.62	0.001	R parietal lobe

inferior temporal and superior parietal cortices and minimal change in the hippocampal formation (Raz *et al.,* 1997). The lack of a substantial age-related change in the amygdala/hippocampal regions demonstrated by our data and work by Raz *et al.* (1997) is somewhat surprising and at odds with other reports. Animal and human pathological studies have demonstrated age-related changes in the hippocampus (Kemper, 2000; Landfield, 2000), as have previous structural imaging studies and recent work using MR spectroscopy (Schuff *et al.,* 1999). A possible explanation for this discrepancy could be the sampling methods used to assess the hippocampus: region of interest techniques used in these previous studies may be observer dependent and subject to error due to the complex and variable shape of the hippocampus. It should be noted that we used VBM to examine age-related changes in local tissue composition, deliberately adjusting for macroscopic and shape differences that classical ROI-based morphometric approaches characterise. It is also worth emphasizing that our data are reporting regionally specific changes within the grey matter compartment over and above global grey matter change, whereas most other studies report changes without covarying out global grey matter volume. A very recent region of interest and voxel-wise morphometry paper in young adults reported that the volume of the amygdala appeared to be independent of age and gender, whereas the hippocampi showed shrinkage with age in men but not in women (Pruessner *et al.,* 2001). The statistical model used in this paper did however not model the global amount of grey matter and the age range is substantially different, so it cannot be directly compared with our method.

Sex Differences

The whole brain volume and grey and white matter partitions were larger in males compared with females in accordance with previous literature (Raz *et al.,* 1997; Coffey *et al.,* 1998; Gur *et al.,* 1991; Murphy *et al.,* 1996).

(modulated) positive correlation with age. Regional areas of relative preservation of grey matter volume from 465 normal subjects superimposed on a normalized structural image in the coronal plane. The color bar represents the *T* score. Significant voxels ($P < 0.025$ corrected) are noted bilaterally in amygdala/hippocampal complexes, entorhinal cortex, and lateral thalami. The second figure shows positive (in red) and negative (green) correlations superimposed on the same structural image. (d) Grey matter concentration: (unmodulated) positive correlation with age. Regions of relative preservation of grey matter concentration from 465 normal subjects superimposed on the whole brain template derived from all subjects. The color bar represents the *T* score. Significant voxels ($P < 0.025$ corrected) are noted bilaterally in the thalami.
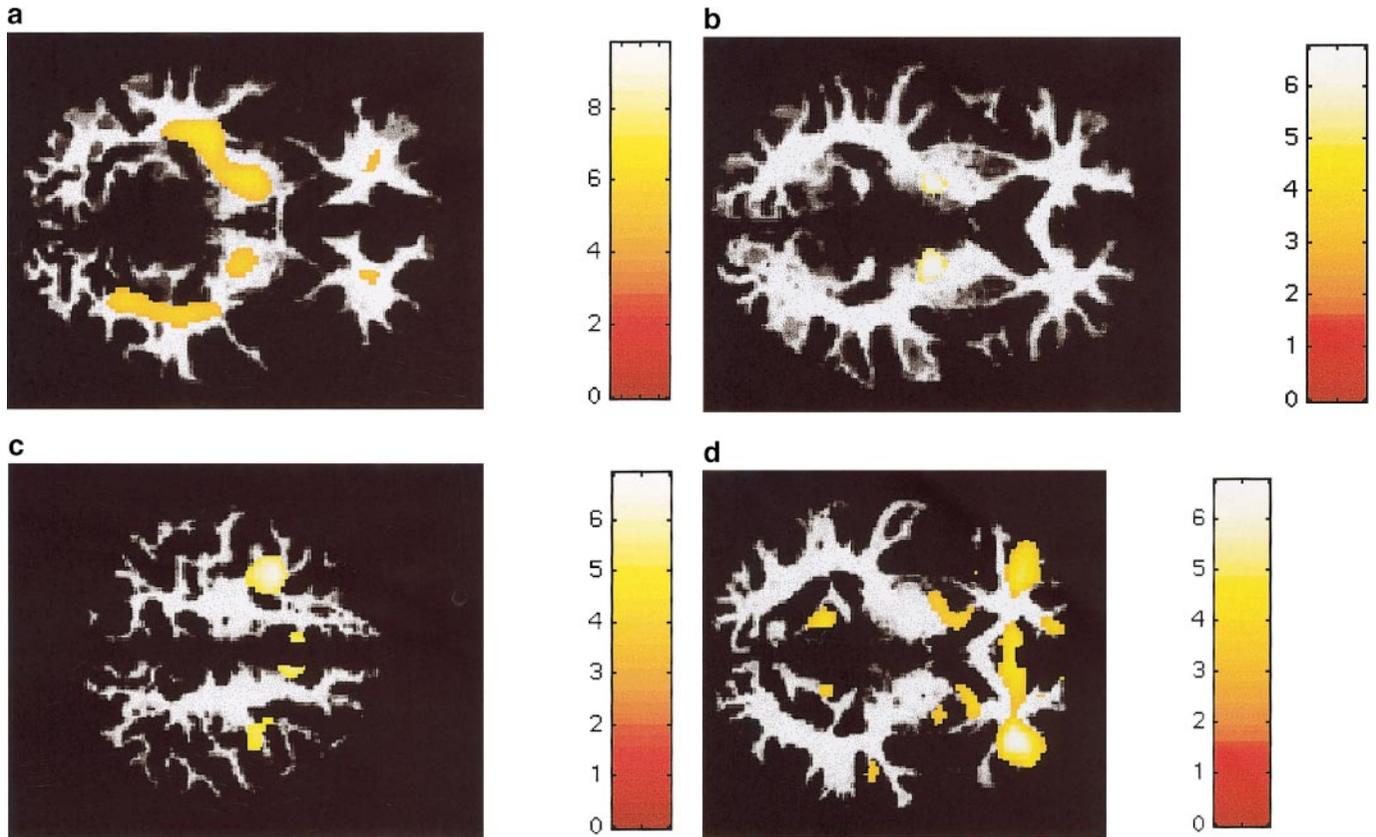
FIG. 5. (a) White matter volume: (modulated) negative correlation with age. Regions of accelerated loss of white matter volume from 465 normal subjects superimposed on a normalized white matter axial image from one of the subjects. The colour bar represents the T score. Significant voxels are seen bilaterally in the corona radiata, bordering on ventral thalamus (voxels classified as white matter), and frontal white matter. (b) White matter concentration: (unmodulated) negative correlation with age. Regions of accelerated loss of white matter concentration from 465 normal subjects superimposed on a normalized white matter axial image from one of the subjects. The color bar represents the T score. Significant voxels are seen bilaterally posterior limbs of the internal capsules, bordering on lateral thalamus (lateral thalamus voxels are segmented partially as grey matter and partially as white matter). (c) White matter volume: (modulated) positive correlation with age. Regions of relative preservation of white matter volume are superimposed on a normalized segmented white matter axial image of one of the subjects. The color bar represents the T score. Significant voxels ($P < 0.025$ corrected) are seen bilaterally in the frontal white matter. (d) White matter concentration: (unmodulated) positive correlation with age. Regions of relative preservation of white matter concentration from 465 normal subjects superimposed on a normalized white matter axial image from one of the subjects. The colour bar represents the T score. Significant voxels are seen bilaterally in the internal capsules, frontal and posterior temporal white matter.

We observed an interaction of sex with age-related global grey matter decline, with a steeper age-related decline in males, in accordance with previous reports (Cowell *et al.,* 1994; Gur *et al.,* 1991; Murphy *et al.,* 1996; Oguro *et al.,* 1998; Xu *et al.,* 2000), although this effect was not significant when global grey matter was expressed as a fraction of TIV. We did not observe any interaction of sex with regional grey matter volume or concentration, contrary to Murphy *et al.* (1996) who showed greater age related loss in frontal and temporal lobes in males, and greater loss in hippocampus and parietal lobes in females. There was no significant interaction of sex with age for CSF or white matter change either globally or regionally. Some previous studies have found greater increases in CSF spaces in males compared with females (e.g., Coffey *et al.,* 1998; Gur *et al.,* 1991), although this has not been reproduced by others (Guttman *et al.,* 1998).

Many previous reports have suggested regional sex differences in age-related decline, for example, Raz *et al.* (1997), demonstrated a steeper trend of ageing in the inferior temporal cortex in males. Xu *et al.* (2000), showed significantly more atrophy in posterior right frontal lobe, right temporal lobe, left basal ganglia, parietal lobe, and cerebellum in males, using semiautomated region of interest MR techniques in 331 subjects, but without partitioning the brain into grey and white matter. Salat *et al.* (1997) showed sex differences in the corpus callosum with ageing, but no atrophy of the pons or cerebellum. Gunning-Dixon *et al.* (1998) showed differential shrinkage of the globus pallidus in males. Murphy *et al.* (1996) reported sex differences in the ageing pattern of whole brain, frontal, temporal and parietal lobes, and hippocampus. We find it difficult to compare the results of these studies with our own, particularly since the majority of these studies
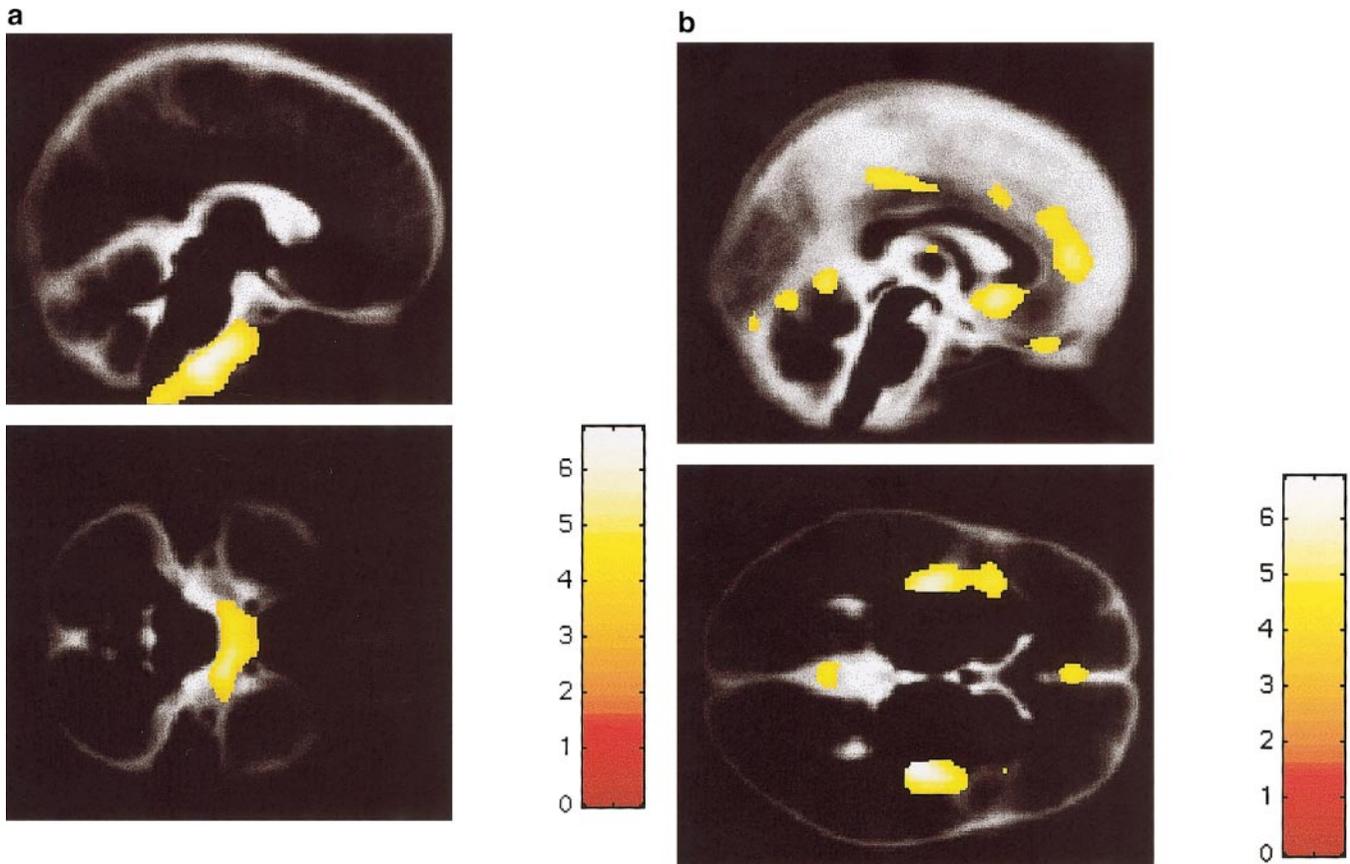
FIG. 6. (a) CSF volume: (modulated) negative correlation with age. Regions of relatively little enlargement of the CSF space from 465 normal subjects superimposed on a mean normalized CSF image from the group, in sagittal and axial planes. The color bar represents the T score. Significant voxels are seen in the pontine cistern. (b) CSF volume: (modulated) positive correlation with age. Regions of relative accelerated enlargement of the CSF space from 465 normal subjects superimposed on a mean normalized CSF image from the group, in midsagittal and axial planes. The color bar represents the T score. Significant voxels are seen in the Sylvian and interhemispheric fissures; chiasmatic and supra cerebellar cisterns; cisterna magna and third ventricle.

are confounded to a greater or lesser degree by methodological factors such as normalizing for brain size, region of interest measurements, quality of structural images, and the use of manual segmentation techniques.

Methodological Issues

Voxel-based morphometry is a fully automated whole brain technique that detects regionally specific differences in brain tissue composition on a voxel by voxel basis. At its simplest, it involves a voxel-wise comparison of the local concentration of grey matter between two groups of subjects (Ashburner and Friston, 2000). In order for VBM to be valid a number of assumptions need to hold. All raw original structural images need to be acquired on the same scanner with identical imaging parameters, since different acquisitions can result in intensity and geometric variations, and this has particular relevance in longitudinal studies. If such variations are systematic they can emerge erroneously as group differences. In this study all subjects were scanned on the same scanner using identical

imaging parameters and the scanner was subject to strict quality control. The templates were created from a subset of the group, which matched the mean age, age-range, and sex of the group in order to avoid bias during the spatial normalization step. The nonlinear spatial transformations used in this study do not attempt to match every gyrus in the brain exactly, rather the goal is to accommodate global brain shape differences. If the spatial normalization were perfect, then we would detect no structural differences in the normalized images, and all the differences would be in the deformation fields, and would be tested using TBM. The drawback of the TBM option is the requirement of high dimensional warps, which are computer intensive and time consuming. By applying the modulation step we incorporate information from the deformation fields and are in effect moving more toward TBM, and while this current approach cannot provide exact matches between small cortical or deep grey matter structures, it provides additional information in a practical way for large subject cohorts. The segmentation step needs to correctly identify grey and white matter and CSF par-

titions. In areas where grey/white matter differentiation is poor, for example, in the brainstem and thalamus, voxels may be incorrectly classified, even using an optimal preprocessing method. This effect is demonstrated in the significant lateral thalamic differences we detected on both the grey and white matter analyses (Figs. 4c, 4d, 5a, and 5b). These age-related differences are real and significant but their cause cannot be attributed directly to grey/white matter changes, rather in the way these changes impact on the classification as grey or white. We are currently attempting to address this problem by optimizing the MR structural imaging sequence to provide better grey/white matter contrast and segmentation (Deichmann *et al.,* 2000). Additional improvements can be made to the segmentation procedure by the creation of customised prior probability maps appropriate to the subject group of interest. This has particular relevance when studying patient populations whose brain structure differs greatly from young normal subjects. We included elderly subjects with a few small white matter hyperintensities. In addition perivascular spaces enlarge with age and there may be subtle signal changes more diffusely in the white matter of elderly subjects. These could be potentially misclassified as CSF or grey matter, leading to a potential overestimation of CSF and grey matter and an underestimation of white matter. Since we did not observe global white matter atrophy with age, we can conclude that perivascular spaces and small white matter lesions were predominantly classified as white matter. The inclusion or exclusion of the modulation step facilitates the assessment of *absolute amount* or *concentration* of a region of tissue. The latter does not however provide information about cytoarchitectural structure such as neuronal packing or cell morphometry, hence the term concentration is preferred to density.

The statistics used to identify structural differences assume that the residuals after fitting the model are normally distributed. If the data are not well behaved, it may be appropriate to perform nonparametric statistical analyses (Ashburner and Friston, 2000; Holmes *et al.,* 1996). The voxel-based extent statistic available within SPM, should not be used in VBM. This statistic is based upon the number of connected voxels in a cluster defined by a prespecified threshold. In order to be valid, this test requires the smoothness of the residuals to be spatially invariant, but this is not the case with neuroanatomy which has a highly nonstationary nature and thus leads to inexact p values (Ashburner and Friston, 2000; Worsley *et al.,* 1999).

There is a great deal of endogenous variability within and between brain regions, and in a recent paper the authors report that 80% of the total variance in gyral volume arises from individual and specific gyri, while only 10% of the total variance reflects uniform scaling to total neocortical volume (Kennedy *et al.,* 1998). In addition there can be contributions from artifactual sources such as imperfections in the spatial normalization that themselves show a regional specificity. This has implications for the sensitivity of any morphometric technique to detect changes in regions of high variance. Our technique may be relatively insensitive to subtle age effects in regions of high variance while more sensitive to change in regions of low variance; however, this is the point of using SPM that employs a regionally specific estimate of variance. This regional variance may well explain the inconsistency of the literature with regard to regionally specific age changes, especially in small brain structures. The hippocampus for example, is a relatively small structure with a complex architecture, which often demonstrates a degree of variability between subjects on visual inspection. VBM has demonstrated subtle changes within the hippocampus in a group of taxi-drivers, that corroborated independent and accurate ROI measurements (Maguire *et al.,* 2000), suggesting that this technique can register and segment small structures with some degree of accuracy. There is the potential for error in patients, for example those with Alzheimer's disease or indeed in normal elderly subjects, since the grey/white matter contrast is reduced, and segmentation may be less accurate. As high dimensional warping techniques advance to the stage where they can provide accurate mapping of small gyri in large subject groups in a time efficient and practical way, then some of these issues will be resolved.

Conclusion

Our data provide evidence of specific patterns in the structural brain correlates of ageing, not only globally between grey and white matter compartments, but also locally within regions of the brain. The use of large numbers of subjects in this study permitted the examination of relatively subtle age-related effects, but also highlighted the need for a rigorous and optimal VBM method to avoid errors of interpretation caused by misclassification of non-brain voxels. Significantly they have been obtained with a fully automated method that eschews observer bias and the data have been obtained in life, eliminating post mortem and agonal changes. They also speak to VBM as a tool for detecting subtle structural brain changes in normal subjects.

REFERENCES

Adachi, T., Kobayashi, S., Yamaguchi, S., and Okada, K. 2000. MRI findings of small subcortical "lacunar-like" infarction resulting from large vessel disease. *J. Neurol.* **247:** 280–285.

Ansari, K., and Loch, J. 1975. Decreased myelin basic protein content of the aged human brain. *Neurology* **25:** 1045–1050.

Ashburner, J., Neelin, P., Collins, D., Evans, A., and Friston, K. J. 1997. Incorporating prior knowledge into image registration. *NeuroImage* **6:** 344–352.

Ashburner, J., Hutton, C., Frackowiak, R. S. J., Johnsrude, I., Price, C., and Friston, K. J. 1998. Identifying global anatomical differences: Deformation-based morphometry. *Hum. Brain Mapp.* **6:** 348–357.

Ashburner, J., and Friston, K. J. 1999. Nonlinear spatial normalization using basis functions. *Hum. Brain Mapp.* **7:** 254–266.

Ashburner, J., Andersson, J. L., and Friston, K. J. 2000. Image registration using a symmetric prior—In three dimensions. *Hum. Brain Mapp.* **9:** 212–225.

Ashburner, J., and Friston, K. J. 2000. Voxel-based morphometry—The methods. *Neuroimage* **11:** 805–821.

Buchel, C., Wise, R. J., Mummery, C. J., Poline, J. B., and Friston, K. J. 1996. Nonlinear regression in parametric activation studies. *Neuroimage* **4:** 60–66.

Celsis, P. 2000. Age-related cognitive decline, mild cognitive impairment or preclinical Alzheimer's disease? *Ann. Med.* **32:** 6–14.

Christensen, G. E., Joshi, S. C., and Miller, M. I. 1997. Volumetric transformation of brain anatomy. *IEEE Trans. Med. Imag.* **16:** 864–877.

Coffey, C. E., Lucke, J. F., Saxton, J. A., Ratcliff, G., Unitas, L. J., Billig, B., and Bryan, R. N. 1998. Sex differences in brain ageing: A quantitative magnetic resonance imaging study [published erratum appears in *Arch. Neurol.* 1998. 55(5):627]. *Arch. Neurol.* **55:** 169–179.

Cowell, P. E., Turetsky, B. I., Gur, R. C., Grossman, R. I., Shtasel, D. L., and Gur, R. E. 1994. Sex differences in ageing of the human frontal and temporal lobes. *J. Neurosci.* **14:** 4748–4755.

Davatzikos, C., Vaillant, M., Resnick, S. M., Prince, J. L., Levotsky, S., and Bryan, R. N. 1996a. A computerised approach for morphological analysis of the corpus callosum. *J. Comput. Assist. Tomogr.* **20:** 88–97.

Davatzikos, C. 1996b. Spatial normalization of 3D brain images using deformable models. *J. Comput. Assist. Tomogr.* **20:** 656–665.

Davatzikos, C. 1998. Mapping of image data to stereotaxic spaces: Applications to brain mapping. *Hum. Brain Mapp.* **6:** 334–338.

Deichmann, R., Good, C. D., Ashburner, J., Josephs, O., and Turner, R. 2000. Optimization of 3-D MP-RAGE sequences for structural brain imaging. *NeuroImage* **12:** 112–127.

Evans, A. C., Kamber, M., Collins, D., and Macdonald, D. 1994. An MRI-based probabilistic atlas of neuroanatomy. In *Magnetic Resonance Scanning and Epilepsy* (S. Shorvon, D. Fish, F. Andermann, G. Bydder, and H. Stefan, Eds.), pp. 263–274, Plenum, New York.

Fein, G., Van Dyke, C., Davenport, L., Turetsky, B., Brant-Zawadzki, M., Zatz, L., Dillon, W., and Valk, P. 2000. Preservation of normal cognitive functioning in elderly subjects with extensive white-matter lesions of long duration. *Arch. Gen. Psychiatry* **47:** 220–223.

Filipek, P., Richelme, C., Kennedy, D., and Caviness, V. J. 1994. The young adult human brain: An MRI-based morphometric analysis. *Cerebral Cortex* **4:** 344–360.

Flood, D., and Coleman, P. 1988. Neuron numbers and size in ageing brain: Comparison of human, monkey and rodent data. *Neurobiol. Ageing* **9:** 453–463.

Fox, N., and Freeborough, P. 1996. Visualization and quantification of rates of atrophy in Alzheimer's disease. *Lancet* **348:** 94–97.

Freeborough, P. A., and Fox, N. C. 1998. Modelling brain deformations in Alzheimer disease by fluid registration of serial 3D MR images. *J. Comput. Assist. Tomogr.* **22:** 838–843.

Friston, K. J., Holmes, A. P., Worsley, K., Poline, J.-B., Frith, C. D., and Frackowiak, R. S. J. 1995a. Statistic parametric maps in functional imaging: A general linear approach. *Hum. Brain Mapp.* **2:** 189–210.

Friston, K. J., Holmes, A. P., Poline, J.-B., Price, C. J., and Frith, C. D. 1995b. Detecting activations in PET and fMRI. *NeuroImage* **4:** 223–235.

Guimond, A., Meunier, J., and Thirion, J. P. 2000. Average brain models: A convergence study. *Comp. Vision Image Understand* **77:** 192–210.

Gunning-Dixon, F. M., Head, D., McQuain, J., Acker, J. D., and Raz, N. 1998. Differential ageing of the human striatum: a prospective MR imaging study. *Am. J. Neuroradiol.* **19:** 1501–1507.

Gur, R. C., Mozley, P. D., Resnick, S. M., Gottlieb, G. L., Kohn, M., Zimmerman, R., Herman, G., Atlas, S., Grossman, R., and Berretta, D. 1991. Gender differences in age effect on brain atrophy measured by magnetic resonance imaging. *Proc. Natl. Acad. Sci. USA* **88:** 2845–2849.

Guttmann, C. R., Benson, R., Warfield, S. K., Wei, X., Anderson, M. C., Hall, C. B., Abu-Hasaballah, K., Mugler, J. P., III, and Wolfson, L. 2000. White matter abnormalities in mobility-impaired older persons. *Neurology* **54:** 1277–1283.

Guttmann, C. R., Jolesz, F. A., Kikinis, R., Killiany, R. J., Moss, M. B., Sandor, T., and Albert, M. S. 1998. White matter changes with normal ageing. *Neurology* **50:** 972–978.

Holmes, A. P., Blair, R. C., Watson, J. D. G., and Ford, I. 1996. Nonparametric analysis of statistic images from functional mapping experiments. *J. Cereb. Blood Flow Metab.* **16:** 7–22.

Jernigan, T. L., Archibald, S. L., Berhow, M. T., Sowell, E. R., Foster, D. S., and Hesselink, J. R. 1991. Cerebral structure on MRI, Part I: Localization of age-related changes. *Biol. Psychiatry* **29:** 55–67.

Kemper, T. 2000. Neuroanatomical and neuropathological changes during ageing and dementia. In *Clinical Neurology of Ageing* (M. Albert and E. Knoepfel, Eds.), pp. 3–67, Oxford Univ. Press, New York.

Kennedy, D. N., Lange, N., Makris, N., Bates, J., Meyer, J., and Caviness, V. S., Jr. 1998. Gyri of the human neocortex: An MRI-based analysis of volume and variance. *Cerebral Cortex* **8:** 372–384.

Landfield, P. W. 1988. Hippocampal neurobiological mechanisms of age-related memory dysfunction. *Neurobiol. Ageing* **9:** 571–579.

Last, R. J., and Tompsett, D. H. 1953. Casts of cerebral ventricles. *Br. J. Surg.* **40:** 525–543.

Leary, S. M., Brex, P. A., MacManus, D. G., Parker, G. J., Barker, G. J., Miller, D. H., and Thompson, A. J. 2000. A (1)H magnetic resonance spectroscopy study of ageing in parietal white matter: Implications for trials in multiple sclerosis. *Magn. Reson. Imag.* **18:** 455–459.

Lim, K. O., Zipursky, R. B., Watts, M. C., and Pfefferbaum, A. 1992. Decreased gray matter in normal ageing: An *in vivo* magnetic resonance study. *J. Gerontol.* **47:** B26–B30.

Luft, A. R., Skalej, M., Schulz, J. B., Welte, D., Kolb, R., Burk, K., Klockgether, T., and Voight, K. 1999. Patterns of age-related shrinkage in cerebellum and brainstem observed in vivo using three-dimensional MRI volumetry. *Cereb. Cortex* **9:** 712–721.

Maguire, E. A., Gadian, D. G., Johnsrude, I. S., Good, C. D., Ashburner, J., Frackowiak, R. S. F., *et al.* 2000. Navigation-related structural change in the hippocampi of taxi drivers. *Proc. Natl. Acad. Sci. USA* **97:** 4398–4403.

Meier-Ruge, W., Ulrich, J., Brühlmann, M., and Meier, E. 1992. Age-related white matter-atrophy in the human brain. *Ann. N.Y. Acad. Sci.* **673:** 260–269.

Messert, B. 1972. Reevaluation of the size of the lateral ventricles of the brain: Postmortem study of an adult population. *Neurology* **22:** 941–951.

Miller, A., Alston, R., and Corsellis, J. A. N. 1980. Variation with age in the volumes of gray and white matter in the cerebral hemi-

spheres in man: Measurements with an image analyzer. *Neuropathol. Appl. Neurobiol.* **6:** 119–132.

Miller, A., and Corsellis, J. 1977. Evidence for a secular increase in human brain weight over the past century. *Ann. Hum. Biol.* **4:** 253–257.

Murphy, D. G., DeCarli, C., McIntosh, A. R., Daly, E., Mentis, M. J., Pietrini, P., Szczepanik, J., Schapiro, M. B., Grady, C. L., Horwitz, B., and Rapoport, S. I. 1996. Sex differences in human brain morphometry and metabolism: An *in vivo* quantitative magnetic resonance imaging and positron emission tomography study on the effect of ageing. *Arch. Gen. Psychiatry* **53:** 585–594.

Oguro, H., Okada, K., Yamaguchi, S., and Kobayashi, S. 1998. Sex differences in morphology of the brain stem and cerebellum with normal ageing. *Neuroradiology* **40:** 788–792.

Pfefferbaum, A., Mathalon, D. H., Sullivan, E., Rawles, J., Zipursky, R., and Lim, K. O. 1994. A quantitative magnetic resonance imaging study of changes in brain morphology from infancy to late adulthood. *Arch. Neurol.* **51:** 874–887.

Pfefferbaum, A., Lim, K. O., Zipursky, R. B., Mathalon, D. H., Rosenbloom, M. J., Lane, B., Ha, C. N., and Sullivan, E. V. 1992. Brain gray and white matter volume loss accelerates with ageing in chronic alcoholics: A quantitative MRI study. *Alcohol Clin. Exp. Res.* **16:** 1078–1089.

Pruessner, J. C., Collins, D. L., Pruessner, M., and Evans, A. C. Age and gender predict volume decline in the anterior and posterior hippocampus in early adulthood. *J. Neurosci.* **21:** 194–200.

Raz, N., Torres, I. J., Spencer, W. D., and Acker, J. D. 1993. Pathoclysis in ageing human cerebral cortex: Evidence from *in vivo* MRI investigation. *Psychobiology* **21:** 151–160.

Raz, N., Gunning, F. M., Head, D., Dupuis, J. H., McQuain, J., Briggs, S. D., Loken, W. J., Thornton, A. E., and Acker, J. D. 1997. Selective ageing of the human cerebral cortex observed *in vivo*: Differential vulnerability of the prefrontal gray matter. *Cereb. Cortex* **7:** 268–282.

Resnick, S., Goldszal, A., Davatzikos, C., Golski, S., Kraut, M., Metter, E., Bryan, R. N., and Zonderman, A. 2000. One-year age changes in MRI brain volumes in older adults. *Cereb. Cortex* **10:** 464–472.

Rypma, B., and D'Esposito, M. 2000. Isolating the neural mechanisms of age-related changes in human working memory. *Nat. Neurosci.* **3:** 509–515.

Sachdev, P., Brodaty, H., Rose, N., and Cathcart, S. 1999. Schizophrenia with onset after age 50 years. 2: Neurological, neuropsychological and MRI investigation. *Br. J. Psychiatry* **175:** 416–421.

Salat, D., Ward, A., Kaye, J. A., and Janowsky, J. S. 1997. Sex differences in the corpus callosum with ageing. *Neurobiol. Ageing* **18:** 191–197.

Schretlen, D., Pearlson, G. D., Anthony, J. C., Aylward, E. H., Augustine, A. M., Davis, A., and Barta, P. 2000. Elucidating the contributions of processing speed, executive ability, and frontal lobe volume to normal age-related differences in fluid intelligence. *J. Int. Neuropsychol. Soc.* **6:** 52–61.

Schuff, N., Amend, D. L., Knowlton, R., Norman, D., Fein, G., and Weiner, M. W. 1999. Age-related metabolite changes and volume loss in the hippocampus by magnetic resonance spectroscopy and imaging. *Neurobiol. Ageing* **20:** 279–285.

Schwartz, M. 1985. Computed tomographic analysis of brain morphometrics in 30 healthy adults ages 21 to 81 years. *Ann. Neurol.* **17:** 146–157.

Thompson, P. M., MacDonald, D., Mega, M. S., Holmes, C. J., Evans, A. C., and Toga. 1997. Detection and mapping of abnormal brain structure with a probabilistic atlas of cortical surfaces. *J. Comput. Assist. Tomogr.* **21:** 567–581.

Vargha-Khadem, F., Watkins, K. E., Price, C. J., Ashburner, J., Alcock, K. J., Connelly, A., *et al.* 1998. Neural basis of an inherited speech and language disorder. *Proc. Natl. Acad. Sci. USA* **95:** 12695–12700.

Wahlund, L. O., Agartz, I., Almqvist, O., Basun, H., Forssell, L., Saaf, J., and Wetterberg, L. 1990. The brain in healthy aged individuals. *Radiology* **174:** 675–679.

Worsley, K. J., Marrett, S. N. P., Vandal, A. C., Friston, K. J., and Evans, A. C. 1996. A unified statistical approach for determining significant voxels in images of cerebral activation. *Hum. Brain Mapp.* **4:** 58–73.

Worsley, K. J., Andermann, M., Neelin, P., Vandal, A. C., Friston, K. J., and Evans, A. C. 1999. Detecting changes in non-isotropic images. *Hum. Brain Mapp.* **8:** 98–101.

Xu, J., Kobayashi, S., Yamaguchi, S., Iijima, K., Okada, K., and Yamashita, K. 2000. Gender effects on age-related changes in brain structure. *Am. J. Neuroradiol.* **21:** 112–118.

Yamano, S., Sawai, N., Minami, S., Nomura, K., Yamamoto, Y., Fukui, R., Takaoka, M., and Dohi, K. 1997. The relationship between brain atrophy and asymptomatic cerebral lesions. *Jpn. J. Geriat.* **34:** 913–919.

Yoshimura, K., and Kurashige, T. 2000. Age-related changes in the posterior limb of the internal capsule revealed by magnetic resonance imaging. *Brain Dev.* **22:** 118–122.